Journal of Power Sources 183 (2008) 330–333

Contents lists available at ScienceDirect

Journal of Power Sources

journal homepage: www.elsevier.com/locate/jpowsour

Short communication

Hydrothermal synthesis of MoO_3 nanobelts utilizing poly(ethylene glycol)

Ch.V. Subba Reddy[a,*], Edwin H. Walker Jr.[a], Chen Wen[b], Sun-il Mho[c]

[a] Department of Chemistry, Southern University and A&M College, P.O. Box 12566, Baton Rouge, LA 70813, United States
[b] Institute of Materials Science & Engineering, Wuhan University of Technology, Wuhan, China
[c] Division of Energy Systems Research, Ajou University, Suwon 443-749, Republic of Korea

ARTICLE INFO

Article history:
Received 6 April 2008
Received in revised form 28 April 2008
Accepted 1 May 2008
Available online 7 May 2008

Keywords:
MoO_3 sol
Nanobelts
Poly(ethylene glycol)
Lithium battery cathodes

ABSTRACT

Metal oxide nanostructures hold enormous potential for electrochemical applications. While thin films of polymer-modified metal oxide electrodes have been widely investigated, there have been a few studies on polymer-modified nanopowders. We report the synthesis of pure molybdenum trioxide (MoO_3), pristine and aged nanobelts using hydrothermal method with poly(ethylene glycol) (PEG). Scanning electron microscope (SEM) images reveal the nanobelts to have dimensions of 1–5 μm in length and 100–600 nm in diameter. The electrochemical measurements show that PEG-used aged MoO_3 nanobelts have higher specific charge capacity than the PEG-free MoO_3 and PEG-used pristine MoO_3 nanobelts.

1. Introduction

One-dimensional inorganic nanostructured materials were received great attention because of their size- and shape-dependent properties [1]. Nanobelts with a rectangular cross-section are interesting and are expected to be the building blocks for nanodevices [2]. Orthorhombic molybdenum trioxide (α-MoO_3), a wide-gap n-type semiconductive material, is attractive due to its layered crystal structure. The asymmetrical MoO_6 octahedra are interconnected through cornerlinking along [1 0 0] and edge-sharing along [0 0 1] to form double-layer sheets parallel to the (0 1 0) plane. The feeble interactions between the double-layer sheets are mostly van der Waals forces [3]. MoO_3 nanostructures can be used in a wide variety of applications because of their properties as ionic conductors [4], cathodes in rechargeable lithium ion batteries [5], thermoelectric materials [6], in electrochromic devices [7–10]. Various MoO_3 nanostructures, such as nanorods, nanowires, nanobelts, and nanoplatelets, have already been synthesized by a variety of methods such as vapor transportation and hydro/solvothermal treatment [3,11–14]. However, the evolution process of MoO_3 nanostructures still remains challenging to material researchers.

Hydrothermal synthesis is one of the most powerful processes employed in nanochemistry. Especially when exposed to supercritical conditions, many starting materials undergo quite unexpected reactions that are often accompanied by the formation of nanoscopic morphologies, which are not accessible by classical routes. Another benefit from hydrothermal synthesis is the wide variety of parameters that can be chosen and combined: reaction temperatures close to room temperature or above 100 °C, variations in the pH value of the systems, concentration of solvents, introduction and removal of templates and other additives, and the choice of different autoclave geometries [15]. Combinatorial methods might be the suitable approach toward systematization of these parameter fields, however, the problem of subsequent scale-up procedures always remain to be solved after a breakthrough in hydrothermal combinatorial synthesis. If, however, a standard procedure for hydrothermal formation of nanoparticles has been established, then these hydrothermal reactions are outstandingly efficient (almost 100% conversion of the starting material), time-saving, and experimentally effortless, such as the low-cost synthesis of vanadium oxide nanotubes [16]. When planning a hydrothermal synthesis of nanostructures with a distinct anisotropic morphology, it is always convenient to start from an educt with a layered structure, especially when a template is involved.

Many researchers have modified MoO_3 with polyaniline (PANI), polyblends (PVA + PVP), and poly(ethylene oxide) (PEO) [17–19]. Rare reports appear in literature on modifying MoO_3 with

* Corresponding author. Tel.: +1 225 771 3717; fax: +1 225 771 5793.
E-mail address: drsreddy2005@yahoo.com (Ch.V. Subba Reddy).

0378-7753/$ – see front matter © 2008 Elsevier B.V. All rights reserved.
doi:10.1016/j.jpowsour.2008.05.005

poly(ethylene glycol) (PEG). In this article, we report the synthesis of PEG-free MoO_3 nanomaterials from MoO_3 sol and PEG-added MoO_3 nanomaterials using hydrothermal process.

2. Experimental

All chemicals (analytical grade) were purchased from Aldrich and were used with no further purification. The polymer-free MoO_3, polymer-used pristine and aged MoO_3 nanobelts were synthesized from their solutions. $MoO_3{\cdot}nH_2O$ sols were prepared by ion exchange of ammonium heptamolybdate tetrahydrate $(NH_4)_6Mo_7O_{24}{\cdot}4H_2O$ (≥99.0%) through a proton exchange resin. After ion exchange, a clear light-blue MoO_3 sol (pH 2.0) was obtained and modified with poly(ethylene glycol) (MW: 6000 g mol^{-1}) solution. The molar ratio of PEG to MoO_3 sol was 0.5. There were two types of the modified MoO_3 sol. The first one was used immediately after modification ("pristine" solution). The second type of modified MoO_3 sol was stored at room temperature for 15 days in a closed volumetric flask before used ("aged" solution). The modified solutions were stirred for 12 h at room temperature, and then poured into a Teflon-lined autoclave and keep at 180 °C for 4 days in a hot oven. After the hydrothermal reaction, the light blue product was washed with distilled water and dried at 80 °C for 10 h.

Crystallographic information of the samples was investigated with a Bruker D8 Advance X-ray powder diffraction (XRD) spectrometer employed with graphite monochromatized Cu Kα radiation (λ = 1.54187 Å). The diffraction data were collected over the 2θ range from 2° to 70°. Fourier transform infrared (FTIR) absorption spectra of the nanobelts were recorded using a 60-SXB IR spectrometer of 4 cm^{-1} resolution, over a wave number range of 400–4000 cm^{-1}. The morphologies of the resulting products were characterized using a SEM (JSM 6390). The electrochemical property of PEG-free MoO_3, PEG-used pristine, and aged MoO_3 nanobelts was carried with a multichannel galvanostat/potentiostat system (MacPile) by applying a constant current (0.4 mA cm^{-2}) in the potential range of 4.0–1.5 V. Electrochemical cells were prepared using a lithium pellet as negative electrode, a 1 mol dm^{-3} solution of $LiPF_6$ in ethylene carbonate (EC)/dimethyl carbonate (DMC) as an electrolyte, a pellet made of the nanobelts, acetylene black and PTFE in a 75:20:05 ratio as a positive electrode.

3. Results and discussion

The XRD pattern of MoO_3 nanobelts is shown in Fig. 1(a). All the peaks can be indexed to α-MoO_3 (JCPDS card no. 05-0508). The strong diffraction peaks of (0 2 0), (0 4 0), and (0 6 0) planes reveal a layered crystal structure or a highly anisotropic growth of the oxides [5]. The PEG-used pristine MoO_3 nanobelts formed a mixture of orthorhombic α-MoO_3 (JCPDS card no. 05-0508) and hexagonal hydrogen molybdenum oxide hydrate $(H_{4.5}Mo_{5.25}O_{18}(H_2O)_{1.36})$ (JCPDS # 01-083-1176) phases (Fig. 1(b)). In the PEG-used aged MoO_3 nanobelts, only observed orthorhombic peaks of α-MoO_3 (Fig. 1(c)) are suggesting that the hexagonal MoO_3 phase is entirely transformed into the orthorhombic MoO_3 phase.

FTIR spectra of the PEG-free MoO_3, the PEG-used pristine and aged MoO_3 nanobelts are shown in Fig. 2. The PEG-free MoO_3 nanobelts exhibit three main vibration modes in 400–4000 cm^{-1} range. The terminal oxygen symmetry stretching mode (ν_s) of Mo=O and the bridge oxygen asymmetry and symmetry stretching modes (ν_{as} and ν_s) of Mo–O–Mo are at 1003, 872 and 574 cm^{-1}, respectively [18]. When polyethylene glycol was added to MoO_3 sol, all the vibration modes changed remarkably and shifted towards lower wave numbers. The ν_s (Mo=O) shifts from 1003 to 991 cm^{-1}

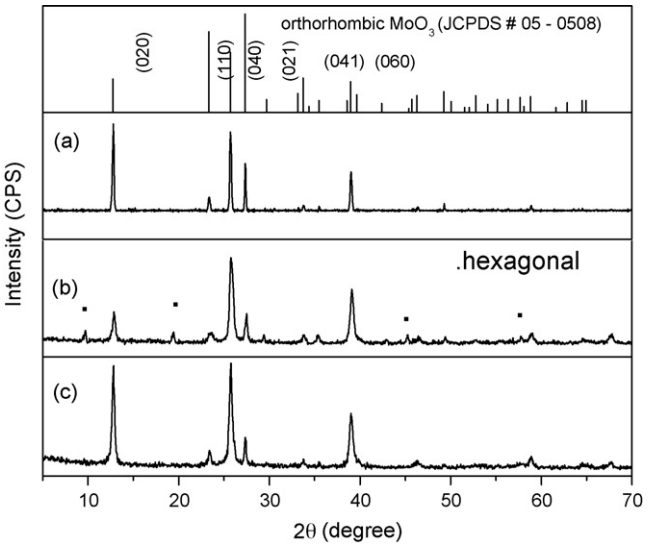

Fig. 1. XRD spectra of (a) the PEG-free MoO_3, (b) the PEG-used pristine MoO_3, and (c) the PEG-used aged MoO_3 nanobelts.

in the PEG-used aged MoO_3 indicating that the Mo=O···H bond is formed in the nanocomposite materials [19]. Namely, the H atoms in the polymer are H-bonded with the O atoms in the Mo=O bonds of MoO_3 sol.

Fig. 3(a)–(c) show the SEM images of the final products of the PEG-free MoO_3 and the PEG-used aged MoO_3 uniformly distributed nanobelts. The nanobelts exhibit a wide range of widths ranging from 100 to 600 nm. The lengths of nanobelts are in the order of 1–5 μm. The nanobelts are straight and have rectangular flat tips with four sharp corners at the upper ends. Smooth facets enclose the surfaces of the nanobelts and from the sharp edges. Coexistence of the nanoparticles and forming hexagonal belts of the PEG-used pristine MoO_3 and a few one-dimensional nanostructures were also observed (Fig. 3(b)).

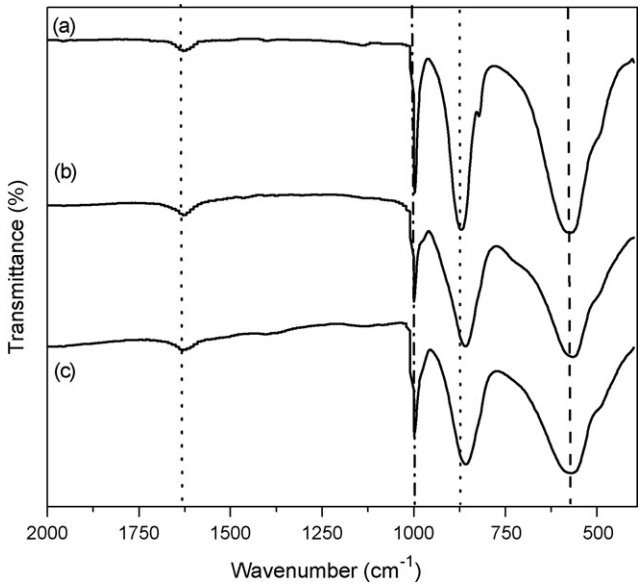

Fig. 2. FTIR spectra of (a) the PEG-free MoO_3, (b) the PEG-used pristine MoO_3, and (c) the PEG-used aged MoO_3 nanobelts.

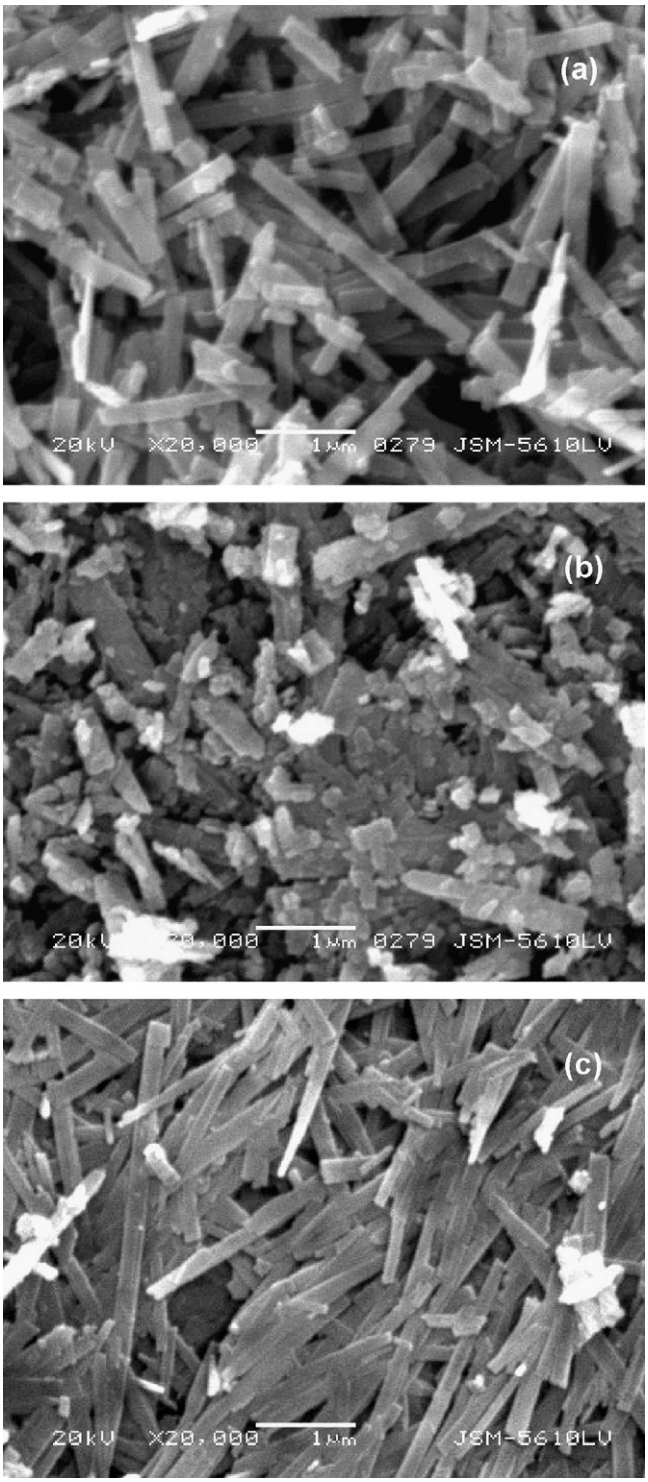

Fig. 3. SEM photographs of (a) the PEG-free MoO_3, (b) the PEG-used pristine MoO_3, and (c) the PEG-used aged MoO_3 nanobelts.

The first discharge curve for the PEG-free MoO_3, the PEG-used pristine and aged MoO_3 nanobelts are given in Fig. 4. Discharge curves show a multi-step process due to structural changes upon the lithium insertion–deinsertion process. This can be confirmed from in situ X-ray patterns of Li_xMoO_3. The discharge capacity of the PEG-used pristine MoO_3 nanobelts battery was lower than that of the PEG-free and the PEG-used aged MoO_3 nanobelts batteries (i.e. 280 mAh g^{-1} in the potential range of 3.25–1.5 V for the as-prepared

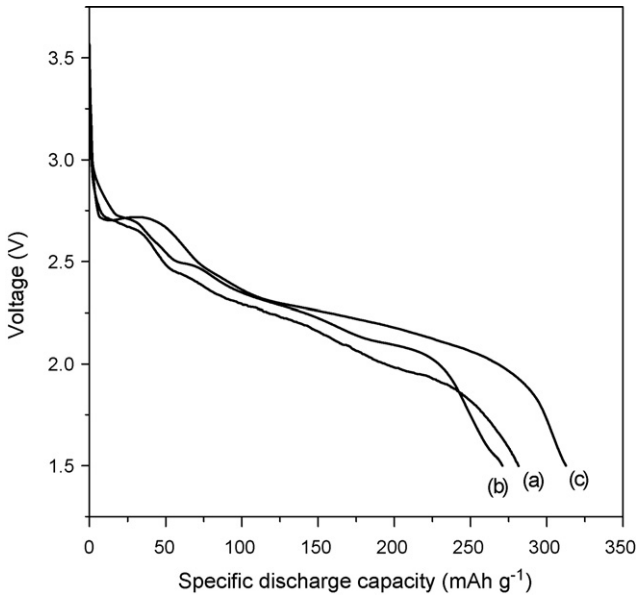

Fig. 4. First discharge curves of (a) the PEG-free MoO_3, (b) the PEG-used pristine MoO_3, and (c) the PEG-used aged MoO_3 nanobelts.

MoO_3 nanobelts, and 271, 313 mAh g^{-1} in the potential range of 3.45–1.5 V for the PEG-used pristine and aged MoO_3 batteries). The decreased capacity in the PEG-used pristine MoO_3 nanobelts battery might be due to a decreased average molybdenum oxidation state or existence of intermediate phase morphology of the nanoparticles and nanobelts. The improved capacity of the PEG-used aged MoO_3 is probably due to the fact that the reduced MoO_3 is partially re-oxidized and polymer chains inside the MoO_3 gallery couple oxidatively from longer chains or with uniform morphology of nanobelts.

Fig. 5 shows the charge–discharge cycles of the PEG-free MoO_3, the PEG-used pristine and aged MoO_3 batteries for 20 cycles. The specific discharge capacity of the PEG-free MoO_3 nanobelts battery after 10 cycles was 240 mAh g^{-1} and the cell exhibited a capacity loss of 14%, demonstrating good cycle stability. The spe-

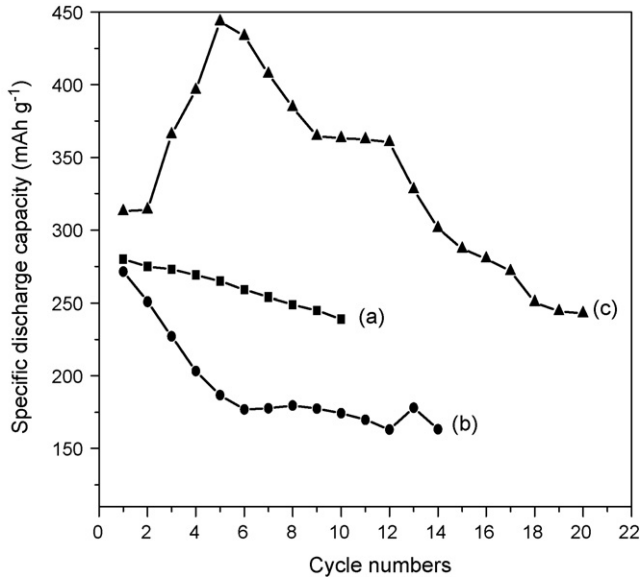

Fig. 5. Cycling property of (a) the PEG-free MoO_3, (b) the PEG-used pristine MoO_3, and (c) the PEG-used aged MoO_3 nanobelts.

Table 1
Comparison of present cathode material performance with earlier reported data

Cathode material	Initial discharge capacity (mAh g^{-1})	Number of cycles	Reference
$Li_{0.99}Mo_{0.01}FePO_4$	161	50	[20]
$MoO_3 \cdot 2H_2O$	490	30	[21]
MoO_{3-x}	279	50	[22]
MoO_3	280	10	Present
Pristine MoO_3 + PEG	271	14	Present
Aged MoO_3 + PEG	313	20	Present

cific discharge capacities of the PEG-used pristine and aged MoO_3 nanobelts batteries after 10 cycles were 175 and 362 mAh g^{-1}, respectively. The capacity loss of pristine battery was of 35% while the capacity gain of 15% was observed in the aged MoO_3 battery. The cycle stability of aged composite materials battery was extended up to 20 cycles (Fig. 5). The capacity loss was of 23% for the PEG-used aged MoO_3 nanobelts battery after 20 cycles. In the polymer-used samples, the ageing plays an important role in activating PEG as an electrochemical active species for lithium insertion. The electrochemical lithium insertion into the MoO_3 framework can be described according to the following reaction:

$$x\mathrm{Li}^+ + x\mathrm{e}^- + [\mathrm{Mo}^{\mathrm{VI}}]\mathrm{O}_3 \leftrightarrow \mathrm{Li}x[\mathrm{Mo}^{(6-x)}]\mathrm{O}_3$$

assuming the reduction from Mo(VI) to Mo(V) and Mo(IV) oxidation states.

Values for the capacity of a number of MoO_3 cathode materials reported earlier along with data for the present cathode materials are given in Table 1. It is clear that the capacities of cells in this paper are comparable with those reported earlier on MoO_3 cathode.

4. Conclusions

The PEG-free and the PEG-used MoO_3 nanobelts were successfully synthesized using hydrothermal process. The electrochemical measurements show that the PEG-used aged MoO_3 nanobelts have higher specific charge capacity than the PEG-free MoO_3 and the PEG-used pristine MoO_3 nanobelts.

Acknowledgments

This research was made possible by grants supplied by the National Science Foundation's Early CAREER program (Cooperative Agreement DMR-0449886) at Southern University. The purchase of the X-ray powder diffractometer was made possible by Grant No. LEQSF(2006-2008)-ENH-TR-68, the purchase of the FTIR was made possible by Grant No. LEQSF(2005-2007)-ENH-TR-65, as well as the purchase of the SEM was made possible by Grant No. LEQSF(2007-2009)-ENH-TR-68, administered by the Louisiana Board of Regents.

References

[1] A.P. Alivisatos, Science 271 (1996) 933.
[2] Z.W. Pan, Z.R. Dai, Z.L. Wang, Science 291 (2001) 1947.
[3] X.W. Lou, H.C. Zeng, Chem. Mater. 14 (2002) 4781.
[4] A. Arulraj, F. Goutenoire, M. Tabellout, O. Bohnke, P. Lacorre, Chem. Mater. 14 (2002) 2492.
[5] W. Li, F. Cheng, Z. Tao, J. Chen, J. Phys. Chem. B 110 (2006) 119.
[6] T. Caillat, J.-P. Fleurial, G.J. Snyder, Solid State Sci. 1 (1999) 535.
[7] P.R. Somani, S. Radhakrishnan, Mater. Chem. Phys. 77 (2002) 117.
[8] P.M.S. Monk, T. Ali, R.D. Patridge, Solid State Ionics 80 (1995) 75.
[9] T.M. McEvoy, K.J. Stevenson, J.T. Hupp, X. Dang, Langmuir 19 (2003) 4316.
[10] U. Bach, D. Corr, D. Lupo, F. Pichot, M. Ryan, Adv. Mater. 14 (2002) 845.
[11] A. Michailovski, J.D. Grunwaldt, A. Baiker, R. Kiebach, W. Bensch, G.R. Patzke, Angew. Chem. Int. Ed. 44 (2005) 5643.
[12] X.M. Wei, H.C. Zeng, J. Phys. Chem. B 107 (2003) 2619.
[13] X.L. Li, J.F. Liu, Y.D. Li, Appl. Phys. Lett. 81 (2002) 4832.
[14] T. Xia, Q. Li, X. Liu, J. Meng, X. Cao, J. Phys. Chem. B 110 (2006) 2006.
[15] K. Byrappa, M. Yoshimura, Handbook of Hydrothermal Technology, Noyes, Park Ridge, NJ, 2001.
[16] M. Niederberger, H.J. Muhr, F. Krumeich, F. Bieri, D. Gnther, R. Nesper, Chem. Mater. 12 (2000) 1995.
[17] O.Yu. Posudievsky, S.A. Biskulova, V.D. Pokhodenko, J. Mater. Chem. 12 (2002) 1446.
[18] Ch.V. Subba Reddy, Y.Y. Qi, W. Jin, Q.Y. Zhu, Z.R. Deng, W. Chen, S.I. Mho, J. Solid State Electrochem. 11 (2007) 1239.
[19] L.Q. Mai, W. Chen, Q. Xu, Q.Y. Zhu, Micro. Eng. 66 (2003) 199.
[20] M. Zhang, Li.F. Jiao, H.T. Yuan, Y.M. Wang, J. Guo, M. Zhao, W. Wang, X.D. Zhou, Solid State Ionics 177 (2006) 3309.
[21] A. Martínez-de la Cruz, I. Juárez Ramírez, J. Power Sources 133 (2004) 268.
[22] H. Ohtsuka, Y. Sakurai, Solid State Ionics 144 (2001) 59.